IEEE Access
Multidisciplinary | Rapid Review | Open Access Journal

IEEE GEOSCIENCE AND REMOTE SENSING SOCIETY SECTION

Received 23 January 2024, accepted 16 February 2024, date of publication 26 February 2024, date of current version 5 March 2024.

Digital Object Identifier 10.1109/ACCESS.2024.3370413

RESEARCH ARTICLE

Increasing the Detection Accuracy of Bi-Temporal Changes via Speckle Whitening of Single-Look Complex Synthetic Aperture Radar Images

LUCIANO ALPARONE[1], FABRIZIO ARGENTI[1], (Senior Member, IEEE), ALBERTO ARIENZO[1,2], AND ANDREA GARZELLI[3], (Senior Member, IEEE)

[1]Department of Information Engineering, University of Florence, 50139 Florence, Italy
[2]OHB System AG, 82234 Weßling, Germany
[3]Department of Information Engineering and Mathematics, University of Siena, 53100 Siena, Italy

Corresponding author: Fabrizio Argenti (fabrizio.argenti@unifi.it)

ABSTRACT This study employs an unsupervised procedure to spatially decorrelate fully-developed speckle in single-look complex (SLC) synthetic aperture radar (SAR) images. The goal is evaluating the extent to which the spatial correlation of the noise induced by the SAR processor affects the detection accuracy of temporal variations of land-cover between two one-look images of the same landscape acquired on different dates. To simulate the scenario, we have spatially correlated a synthetic map of white complex circular symmetric Gaussian noise by using a two-dimensional separable Hamming window in the Fourier domain. The correlated complex speckle field has been modulated by a noise-free optical view, to simulate an SLC SAR image. Subsequently, we have reduced the correlation of the SLC image through a whitening process and calculated the modulus of the complex image. We have applied various methods of statistical change detection for real-valued SAR data, and compared the accuracy of change maps in the following cases: i) ideally uncorrelated noise, ii) correlated noise, iii) correlated noise that has been decorrelated. The study considers three change detection algorithms, ranging from the basic Log-Ratio operator preceded by despeckling to advanced parametric and nonparametric methods based on Kullback-Leibler distance and mean-shift clustering of bivariate scatterplots of local means. Simulation results demonstrate consistent performance improvements, in terms of both geometric accuracy and reduced number of false alarms.

INDEX TERMS Inverse filtering, noise whitening, SAR image change detection, SAR processor, single-look complex (SLC) images, synthetic aperture radar (SAR), tapering windows.

I. INTRODUCTION

The all-weather and all-day acquisition capability makes spaceborne synthetic aperture radar (SAR) systems extremely attractive for environmental monitoring. SAR images, however, are intrinsically affected by speckle, a multiplicative granular noise, typical of coherent imaging systems, that degrades the visual appearance of images and reduces the performance attainable by analysis / processing algorithms.

Fully-developed speckle is characterized in the spatial frequency domain as a white process. In the complex spatial domain (in-phase and quadrature components), it is modeled as a spatially uncorrelated multiplicative random process, independent of the underlying radar reflectivity and characterized by a zero-mean circular Gaussian probability density function (PDF) [1]. During the processing of raw data to create an image, however, there may be stages that violate the validity of this assumption. Before the at-ground SAR processing, the raw data from satellite are slightly oversampled (by approximately 10%) and windowed, that is weighted in the Fourier-domain, where the deconvolution process takes place, to prevent Gibbs effects from occurring around point targets. As a consequence of the use of tapering windows, typically Hamming or Kaiser windows, in both

The associate editor coordinating the review of this manuscript and approving it for publication was Gerardo Di Martino.

the range and azimuth focusing steps, the speckle at the output of the SAR processor, becomes autocorrelated. Thus, the single-look complex (SLC) image is generated with spatially correlated speckle; this was first noted by some authors [2], [3], who adjusted their processing algorithms to tackle correlated speckle. Incoherent spatial multi-looking is a common practice, whenever phase information is not relevant. The benefit of a reduction in spatial correlation, achieved by means of downsampling, however, is paid in terms of a degraded spatial resolution, and hence of a loss of information that may not be tolerable in some applications.

In this work, we investigate the sensitivity of SAR change detection algorithms to the spatial correlation of single-look envelope-detected real-valued speckle patterns. The goal is to achieve an improvement in the change detection performance by means of a whitening of the data, whenever they are available in SLC format. Statistical change analysis is the analysis of *structural* rather than of *stochastic* changes between two scenes represented by single-look data, taken in two dates along parallel orbits by the same satellite or by a satellite constellation (e.g. TerraSAR-X–Tandem-X, COSMO-SkyMed). The spatial resolution of the SLC format is the highest resolution allowed by the SAR system in a preset modality: StripMap, ScanSAR or SpotLight [4]. Such a resolution is highly beneficial for change analysis and should be preserved by pre-processing. Thus, the spatial correlation can be removed by means of a *deconvolution* operation which aims to restore a *flat* SLC power spectrum [5]. The same whitening step has been applied also to interferometric SAR (InSAR) couples [6] with promising results, thanks to the unbiased estimation of interferometric coherence [7] from whitened data. Actually, coherence measures structural and stochastic changes at the same time, because it is related to the similarity of speckle patterns between the scenes [8]. A further achievement of some of the authors is an investigation on the influence of correlation on polarimetric SAR (PolSAR) filtering [9] and features extraction [10]: again, the decorrelation procedure described in the seminal article [5], has been separately applied to all polarimetric channels [9]; quantitative assessments are reported in [10], thanks to the use of a PolSAR simulator. The influence of speckle autocorrelation on SAR change detection has been the object of a preliminary study carried out by some of the authors [11].

In a realistically simulated scenario, we generated uncorrelated SLC data from high-resolution optical images and synthetic patterns of complex speckle. We optionally introduced a spatial correlation in the synthetic SLC data by means of separable Hamming windows along range and azimuth. Then, we removed the correlation by using the whitening procedure [5]. Afterwards, for the three case of uncorrelated, correlated and decorrelated speckle, we extracted the modulus of the SLC images, applied change detection algorithms and compared the accuracy of the estimated change maps for the three cases. Three change detection methods were considered: from the simple Log-Ratio point operator preceded by despeckling [12], to more advanced parametric or nonparametric methods based on Kullback-Leibler divergence [13] or on mean-shift clustering of the bivariate scatterplot [14], respectively. Simulation results show a consistent improvement in performance of the decorrelated vs the correlated case, notably the geometric accuracy of changes [15], but also the detection probability of fake changes, or false-alarm probability [16].

This paper is organized as follows. Section II provides a brief review of SAR systems and explains the origin of speckle correlation and how it can be abated in practical scenarios concerning real-world data. Section III reviews the main approaches for SAR change detection used throughout this work. Section IV presents quantitative results on two simulated datasets portraying an urban and a rural scenario and discusses the assets of decorrelation with respect to the specificity of each change algorithm. Concluding remarks and possible developments are drawn in Section V.

II. SPATIAL DECORRELATION OF SPECKLE

A. OVERVIEW OF SAR SYSTEM

SAR images are computed images obtained by processing radar echoes taken from a moving platform [1], [4]. A train of pulses, or chirps, is sent along a leaning direction across the track of the platform with respect to the vertical, referred to as slant-range. The SAR system records the complex echoes of targets encountered across the track, which are discriminated by the delays of their responses. The in-phase and quadrature components of the complex envelope are sampled at least twice the chirp bandwidth, quantized and accumulated in a buffer; they constitute the 2D array of *raw* data, which is stored in a mass memory of the aircraft or transmitted to the ground station by the satellite.

Afterward, the matrix of raw data, which does not show any perceivable shape, but only a granular noise and a slowly space-varying mean, must be focused by the SAR processor at the ground station, more seldom on the aircraft, never on the satellite, because of processing power requirements. The processing consists of a 2D separable deconvolution: of the nonideal shape of the chirp [17] in the slant-range direction (range focusing) and of the antenna pattern gain, whose shape varies with the range, in the direction along the track of the platform (azimuth focusing). Deconvolution performed in the Fourier domain is fast and accurate, but requires that the trajectory of the platform is perfectly predictable, which happens for a satellite and a large/medium aircraft, but not for a small aircraft or for drones [18].

The two deconvolution operations have the purpose of simulating: a) an ideal perfectly bandlimited pulse having a rectangular Fourier transform; b) an ideal antenna beam, with a narrow main lobe and absence of side lobes in the azimuth direction. After deconvolution, however, the pulse becomes the inverse Fourier transform of a *rect*, that is, a *sinc* function having slowly decaying tails; analogously in the azimuth

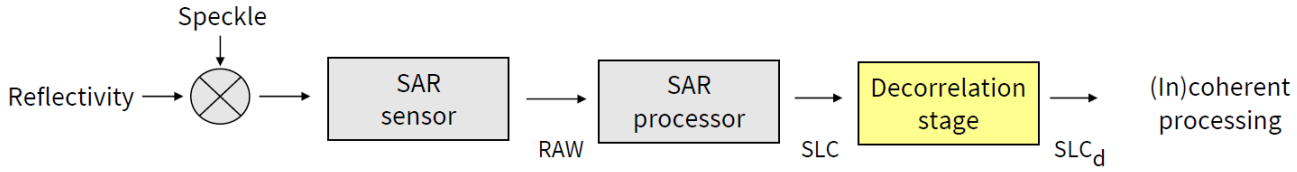

FIGURE 1. Flowchart of SAR system (onboard sensor followed by at-ground processor) with optional whitening stage.

direction, after the antenna pattern has been deconvoluted. The unpleasant consequence is that after deconvolution a target one pixel wide (point target) is surrounded by a square cross with dashed sides, originated by separable Gibbs effects in the two dimensions.

The SAR processor usually employs frequency windowing to prevent the onset of Gibbs effects. Widely used are Hamming and Kaiser windows. The benefit of windowing is avoiding the spread of point targets. The drawback is that fully-developed speckle, which should be perfectly uncorrelated, at least if the raw data are not oversampled, becomes spatially correlated and passes from a *sandy* to a *grainy* appearance. Speckle originates from the coherent combination of echoes from multiple scattering elements at the receiver end. Fully-developed speckle occurs when a significant number of independent scatterers is contained within the resolution cell of the system, approximately twice the pixel size, or four times in terms of areas. If there are few dominant scattering elements in the cell, speckle is not fully-developed and in principle it might even vanish, if a unique scatter, e.g., a corner reflector or a man-made structure, exists in the cell. The autocorrelation function of speckle is expected to impact on the subsequent analysis and processing for statistical change detection from SAR data.

B. PROBLEM STATEMENT

Here, we make use of the spectral properties of SLC SAR images derived in [19]. Accordingly, the observed scene is made-up by a set of scatterers, one for each pixel. Let $S^w_{pq}(r)$ denote the discrete complex scattering coefficient, where the subscripts pq denote the transmitting and receiving polarizations, namely, HH, VV, HV and VH, and $r \triangleq (r_x, r_y)$ denotes the two-dimensional coordinates in the image plane. Under the assumption of fully-developed speckle, $S^w_{pq}(r)$ is a zero-mean, white complex circular symmetric Gaussian process, with variance $\sigma_{pq}(r)$, which is the radar reflectivity imaged by the system [1]. The complex image at the output of a SAR processor equipped with a 2D separable tapering window $H(f)$, with $f \triangleq (f_x, f_y)$, can be formulated as a convolution of the scattering coefficient by the inverse Fourier transform of the frequency tapering window, $H(f)$, or point spread function (PSF), $h(r)$:

$$S_{pq}(r) = S^w_{pq}(r) * h(r) \tag{1}$$

or equivalently in the Fourier domain as:

$$S_{pq}(r) = \mathfrak{F}^{-1}\left\{\mathfrak{F}\left\{S^w_{pq}(r)\right\} \cdot H(f)\right\}. \tag{2}$$

In Eqs. (1) and (2), we have supposed that the entire SAR system, i.e. onboard acquisition followed by at-ground focusing, can be modeled as a cascade of linear shift-invariant filters, characterized by their PSFs.

The most widespread formulation of the SAR image with fully-developed speckle model for the single-polarization case (the subscripts $p = q$ will be omitted, hereafter) is given by:

$$|S(r)|^2 = \sigma(r) \cdot u_u(r) \tag{3}$$

in which $u_u(\boldsymbol{r})$ is the fading term, modeled as a white random process having mean and variance both unity-valued and a negative exponential PDF. Eq. (3) represents the *intensity* format of a single-look image, that is the power of the backscattered signal. Note that, according to its definition [20], the signal-to-noise ratio (SNR) of a single-look SAR image in intensity format is 0 dB. The model (3) holds, if the SAR system features an ideal PSF, i.e. a discrete $\delta(\boldsymbol{r})$ function. The case of polarimetric SAR data is more complex and is not reported here, because the speckle patterns are not independent among the polarimetric channels [21], even though each channel is focused independently of the others.

A more general formulation of the problem accounts for a possible autocorrelation of the fading term and is given by:

$$|S(r)|^2 \approx \sigma(r) \cdot u_s(r) \tag{4}$$

where $u_s(\boldsymbol{r})$ is the fading term, spatially correlated because of the non-ideal SAR system transfer function, and independent of $\sigma(\boldsymbol{r})$. According to [19], the approximation is better verified, the wider the Fourier transform of the SAR system's PSF is than the power spectral density of of the noise-free radar reflectivity. In other words, the correlation length of the speckle should not be greater than that of the reflectivity. The model (4) accounts for the speckle correlation, provided that the bandwidth of the SAR system largely encompasses the power spectrum of the imaged reflectivity.

The rationale of using speckle decorrelation is exactly to remove the effects of the SAR system transfer function, to restore $S^w(\boldsymbol{r})$ from $S(\boldsymbol{r})$. The blind deconvolution problem may be simplified assuming the SAR system's transfer function to be a band-limited lowpass filter with cutoff frequency f_c:

$$H(f) \approx 0 \qquad \forall |f| > |f_c|. \tag{5}$$

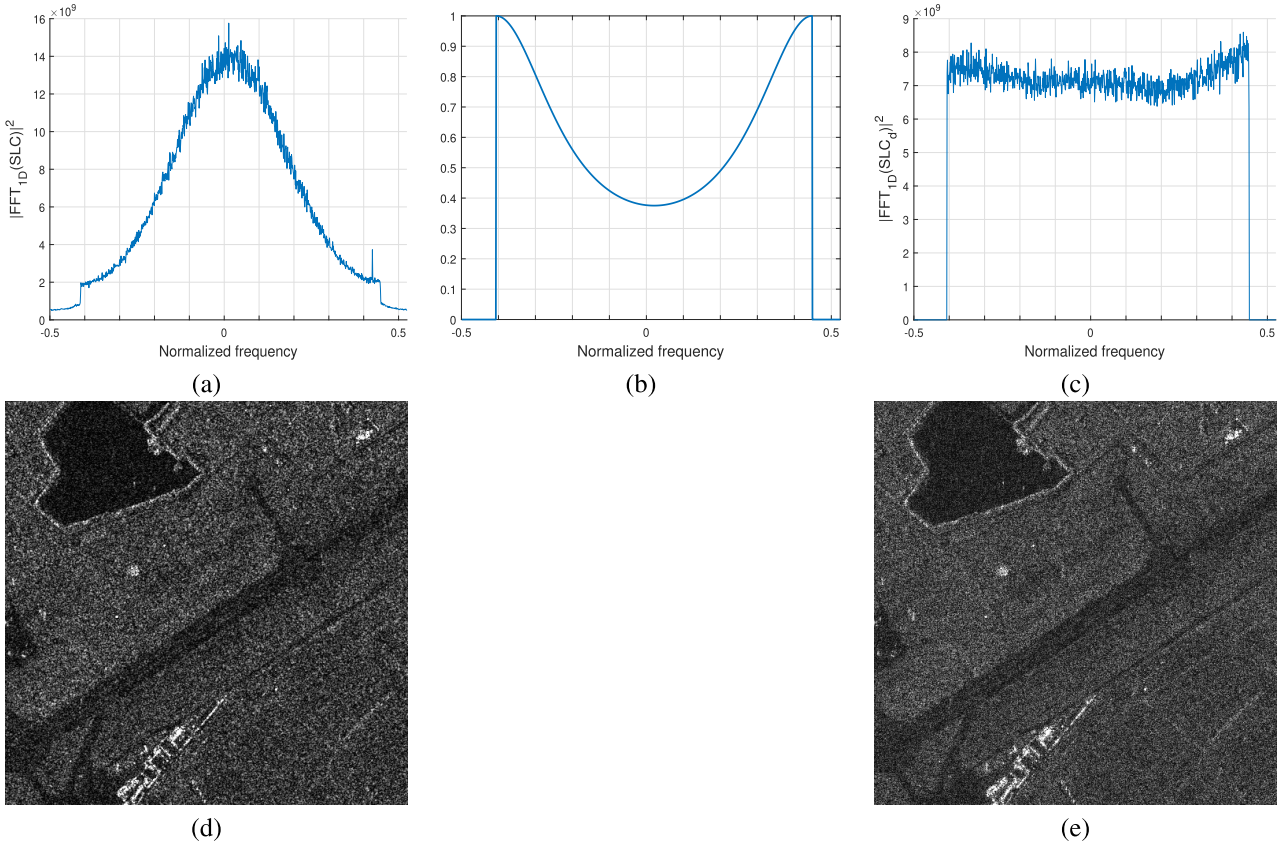

FIGURE 2. (a): Power spectrum of true SLC data (correlated) in slant-range direction; (b): frequency response of inverse filter; (c): power spectrum of correlated SLC data in (a) after decorrelation with the filter in (b); (d) modulus of SLC image with original power spectrum in (a); (d) modulus of SLC image with whitened power spectrum as in (c).

Unlike other image restoration methods, any assumptions on $\sigma(\boldsymbol{r})$ are unnecessary; it can be demonstrated that an estimator of $\hat{S}^w(\boldsymbol{r})$ is given by:

$$\hat{S}^w(r) = \begin{cases} \mathfrak{F}^{-1}\{\mathfrak{F}\{S(r)\} \cdot [\hat{H}(f)]^{-1}\} & \forall |f| \le |f_c| \\ 0 & otherwise \end{cases} \quad (6)$$

in which $\hat{H}(f)$ denotes the estimate of the transfer function $H(f)$.

In this way, the problem of blind deconvolution may be translated to the spectral estimation of the SAR transfer function $H(f)$, required to build the inverse filter and recover the original *whiteness* of the data. Unless $H(f)$ is otherwise known, its estimation may be performed by using an LS minimization in the spectral domain starting from the SLC data [5]. In most practical cases the tapering window is known and need not to be estimated.

Fig. 1 shows the processing chain including the decorrelation stage of the complex data. The cascade of SAR sensor and SAR processor constitutes the SAR system, which in principle should output the product of reflectivity and complex speckle found at its input. In practice the SAR processor includes a tapering window and hence its output becomes spatially correlated and should be decorrelated by means of the inverse filter of the window.

With reference to a true SLC image provided by the X-band COSMO-SkyMed constellation, Fig. 2 shows the range power spectrum after the SAR processor, the inverse filter used by the decorrelation stage and the power spectrum at its output. The moduli of original and whitened images are displayed in Fig. 2(d) and Fig. 2(e), respectively. They exhibit lag-one correlation coefficients (CC) equal to 0.29, before decorrelation and 0.05, after being decorrelated. The original range power spectrum, shown in Fig. 2(b) resembles a Hamming window, as otherwise indicated in the data product manual. The whitened spectrum is approximately flat. Statistical estimations of from local windows of correlated samples may be inaccurate, because the set of samples is not locally ergodic.

C. PROCESSING OF POINT TARGETS

The effectiveness of the whitening process described in Section II-B is obviously reduced if the fully-developed speckle model does not hold; this occurs in the presence of single-pixel reflectors or strong scatterers, referred to as *point targets*. The latter must be removed and replaced with synthetic patches of complex speckle,

with variance proportional to the average variance of neighboring pixels, before the deconvolution process is performed [5].

For single-polarization SAR images, the detection of point targets is carried out through a percentile thresholding of the modulus (amplitude), or squared modulus (intensity) of the SLC image [20]. For PolSAR data, advantage should be taken of the capability of PolSAR to yield information on the nature of the scattering mechanisms [10].

It is note worthy that the Fourier-domain whitening scheme requires a proper point-target detection. The deconvolution process cancels the effects of the tapering window: the spatial correlation is removed over distributed targets, whereas on strong scatterers, or *hard* targets, if they are not detected, removed and replaced, the inverse filter will originate undesired annoying cross-shaped artifacts, similar to the SAR system's PSF, especially due to the increment of the antenna sidelobes in azimuth. Thus, the processing of point targets before the spectrum flattening operation, is crucial. In this sense, rather than a simple thresholding, which works, despite its simplicity, a more refined point-target detector could be adopted. As an example, contextual information on the nature of targets may be used after thresholding the ''brightest'' pixels, because if the target spans more than one pixel, Gibbs effects are not introduced by the inverse filter. However, if bright spots wider than one pixel are removed after whitening and reinserted later, the high heterogeneity of pixels surrounding a target makes their speckles to be little developed [22]; thus, the decorrelation is not relevant and can be avoided.

III. CHANGE DETECTION FROM SAR IMAGES

The discrimination between changed and unchanged pixels in very-high-resolution (VHR) bi-temporal SAR images is a nontrivial task because of the presence of speckle [13]. Actually, two SAR images taken on exactly the same scene, but on different times, may be pixel-by-pixel different because of different speckle patterns and calibration uncertainty. The latter is caused by unreliability of the permanent scatterers and/or corner reflectors, which are used for the relative calibration [23], e.g., to compensate the attenuation of e.m. waves in atmosphere, possibly due to different meteorological conditions on the two passes. Also registration inaccuracies between the two images may appear as temporal changes.

For the challenging case of one-look images, despeckling filters, rather than multilooking, may be suitable for preserving the spatial resolution of single-date images and to improve classification, detection, and parameter estimation. However, they are unable to expedite the discrimination between stochastic changes due to speckles and structural changes in radar reflectivity: the reliable detection of changes, both in level, either intensity or amplitude, and in spatial extent, may be a very hard task.

Although the analysis and processing of SAR data is often based on modeling [24], alternative approaches exploiting learning concepts are promising for texture analysis and classification of forests [25]; For the present case, however, change detection methods that are based on learning require extensive training datasets (pre-/post-event images and related ground truth (GT) maps) that may be hardly available. The training datasets could be simulated from optical images by using correlated speckles with different degrees of development: e.g., full, medium, low, null (point targets). In this case, the algorithm would automatically learn how to tackle speckle correlation. Thus, the accurate synthesis of test images becomes a crucial aspect.

A. LOG-RATIO OPERATOR

Maps of pixel ratios, or better of logarithm of pixel ratios (LR), namely difference in backscatters that have been expressed in decibels (dB). are useful for detecting changes [26] with good preservation of geometric details [27], but limited capabilities of rejecting false alarms [12]. The main drawback of features relying on pixel ratios is that they can capture only changes generated by variations in first-order statistics.

SAR systems measure the radar reflectivity of the surface, defined as the ratio of backscattered to incident power. Speckle is a multiplicative fading term originated by the coherent superposition at the receiver of radar echoes of scattering elements within the same resolution cell of the system. Fully-developed speckle means that there are many independent returns from the same cell. A preliminary stage of speckle reduction, or ''despeckling'', is recommended before computing the LR image. A great number of despeckling filters, mostly adaptive, has been been developed over time [28]. The finite size of the processing window of spatial-domain filters, however, originates outliers that are likely to be mistaken for spatial changes. Such blobs increase with speckle correlation and may lead to gross errors. Though speckle correlation is always a drawback, this inconvenience is mitigated for despeckling filters operating in a shift-invariant multiscale domain [29], [30], [31], [32]. Despeckling is expected to preserve texture features, like [33], used for classification [34] and for merging SAR and optical data [35], [36], [37], [38].

As already mentioned, an intrinsic limitation of the change detector based on ratio of local means is that it the comparison is made only on first-order image statistics. According to the established multiplicative model for detected SAR data [39], a piecewise constant radar cross-section is modulated by a unity-mean texture term and by the unity-mean speckle. Hence, changes at texture level that preserve the mean, will likely not be detected. To overcome this inconvenience, higher order statistics, such as Log-cumulants, have been considered to address the change detection problem [40]. Alternatively, a contextual approach to ratioing has been devised [41]. The presence of an imperfect relative calibration between the two images originates an offset in the response of the LR operator, which can be detected and suppressed before the threshold decision.

B. KULLBACK-LEIBLER DISTANCE

The Kullback-Leibler (KL) divergence between the PDFs, f_X and f_Y, of two random variables X and Y is defined as

$$K(Y|X) = \int_{-\infty}^{+\infty} \log\left[\frac{f_X(x)}{f_Y(x)}\right] \cdot f_X(x)dx. \tag{7}$$

The KL divergence is a measure of how much the PDF of Y diverges from that of X. $K(Y|X)$ is not symmetric, but a symmetric extension may be defined as

$$D(X, Y) = D(Y, X) = K(Y|X) + K(X|Y) \tag{8}$$

which is called KL distance (KLD).

In order to improve the estimation of KLD, a parametric approach has been proposed [13]. Let us assume that the statistics of real-valued envelope-detected SAR images can be modeled by the family of PDFs known as the Pearson system. If we adopt an approximation of KLD based on cumulants, by means of the Edgeworth series expansion of KL (KL_E), the change feature based on KLD, CKLD, denoted as c_{CKLD}, has been finally obtained:

$$c_{CKLD} = \mathrm{KL}_E(X, Y) + \mathrm{KL}_E(Y, X). \tag{9}$$

Since moments up to the fourth order are calculated, (9) provides accurate local PDF distance estimation between two SAR images using a large-size sliding window (greater than or equal to 15×15), with uncommon false-alarm rate capability but limited geometrical accuracy, due to the size of the sliding windows for a reliable estimation of local statistics. The relatively large size of the processing window guarantees a low sensitivity to speckle, whose auto-correlation, however, would require even larger windows, with a consequent unavoidable decrement of geometrical accuracy. As stated by the authors themselves [13], the method does not require any preliminary relative calibration between the two images.

C. MEAN-SHIFT INFORMATION-THEORETIC CHANGE DETECTION

The mean-shift information-theoretic change detection (MS-ITCD) algorithm [14] is based on a pixel feature capable of capturing the structural change between two co-registered real-valued SAR images X_1 and X_2, acquired on different dates. MS-ITCD is robust to the stochastic change that may be originated by speckle and co-registration inaccuracies. The method starts from the scatterplot of the amplitude levels in the two images and applies the mean-shift (MS) algorithm [42] to find the modes of the underlying bivariate distribution.

The information-theoretic approach regards the negative of the logarithm of the probability of a mean pixel level in one image conditional to the mean level of the same pixel in the other image, which would measures the amount of information associated to the pixel change, as a feature measuring the amount of structural change. So, the change is related to the conditional information of couples of symbols emitted by two information sources.

Let $x_1(i, j)$ and $x_2(i, j)$ be the symbols emitted by the two information sources X_1 and X_2, respectively, where $i = 0, \ldots I-1$ and $j = 0, \ldots J-1$ are the spatial coordinates. The mean information of the two sources is given by the entropy, or *auto-information*, $H(X_1)$ and $H(X_2)$. Unless the two sources are statistically independent of one another, a fraction of such an information is common to the two sources. This common part is called *mutual information*, $M(X_1; X_2)$, and is a measure of statistical dependency between X_1 and X_2

$$M(X_1; X_2) = H(X_1) - H(X_1|X_2) \tag{10}$$

or, equivalently,

$$M(X_1; X_2) = M(X_2; X_1) = H(X_2) - H(X_2|X_1) \tag{11}$$

in which $H(X_2|X_1)$ is the conditional entropy of X_2 to X_1 and represents the fraction of $H(X_2)$ that cannot be inferred from the knowledge of the reference source X_1, because it is due to unpredictable variations; analogous relationships hold for $H(X_1|X_2)$, by exchanging the subscripts 1 and 2.

Given the conditional information between $x_2(i, j)$ and $x_1(i, j)$, defined by

$$I(x_2(i, j)|x_1(i, j)) \triangleq -\log\left[p(x_2|x_1)\right] \tag{12}$$

the conditional entropy is the expected value of (12),

$$H(X_2|X_1) \triangleq -\sum_{X_1}\sum_{X_2} p(x_1, x_2)\log\left[p(x_2|x_1)\right] \tag{13}$$

where $p(x_1, x_2)$ and $p(x_2|x_1)$ are the joint probabilities of $x_1(i, j)$ and $x_2(i, j)$ and the conditional probabilities of $x_2(i, j)$ to $x_1(i, j)$, respectively.

The ITCD change features can be computed from the scatterplot of the amplitude levels in the two images, while the meanshift-enforced version, MS-ITCD, is computed similarly after performing a migration of the scatterpoints toward the center of their attracting cluster [42].

The effect of mean shift is that the scatterpoints contained in each bin are moved towards the attracting center corresponding to a mode (relative maximum) of the underlying PDF. Unchanged pixels produce scatterpoints that are likely to be moved towards one of the modes along the main diagonal; conversely, changed pixels will be moved towards one of the modes far apart from the main diagonal. The presence of a relative calibration error between the two images (typical values reported in data product manuals are 2 dB, 3 dB at most) has the effect of rotating the main diagonal and is implicitly tackled by the algorithm.

The main difference of MS-ITCD, originally introduced in [43], from its earlier version, ITCD [44], is that the presence of MS: the MS algorithm starts from the scatterplot of the local means in the two images and finds the local maxima (modes) of the underlying PDF, without explicitly calculating the PDF, but simply considering the scatterpoints contained in a window surrounding the gravity center of the cloud of scatterpoints encompassed by the window at the previous iteration [42]. Each iteration moves the window

FIGURE 3. Dataset 1: (a) first acquisition; (b) second acquisition; (c) change map.

FIGURE 4. Dataset 2: (a) first acquisition; (b) second acquisition; (c) change map.

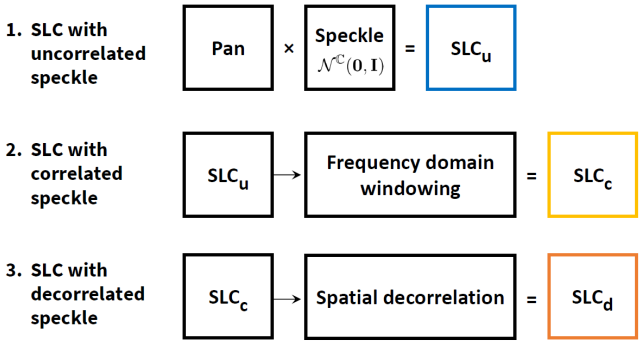

FIGURE 5. Simulation of SLC images with different speckles: uncorrelated, correlated, decorrelated.

towards a cluster in the scatterplot, corresponding to a maximum, either relative or absolute, of the bivariate PDF. The information-theoretic change feature is calculated from the values of conditional probabilities calculated from the off-diagonal modes of the joint PDF. MS-ITCD is slightly more accurate than ITCD [14], but substantially similar. Unlike LR, MS-ITCD and ITCD exhibit good tolerance to speckle and require no preliminary de-speckling, which may introduce an undesired correlation. Nevertheless, the benefits of speckle decorrelation are still evident.

We wish to remind that all the change-detection methods addresses in this study concern single-polarization images. Change detection from polarimetric SAR (PolSAR) data is a more complex task, because of the interrelationships among the various channels. Nevertheless, the information-theoretic approach is still pursued [45].

IV. RESULTS

A. SETUP

Two different datasets have been simulated following the fully-developed speckle model. The first image represents an urban scenario. The second scene portrays a rural landscape. For each dataset, starting from a high-resolution panchromatic (Pan) image from IKONOS satellite, with 1 m^2 spatial resolution and 11 bits radiometric resolution, simulating the noise-free radar reflectivity, first the synthetic reflectivity image with simulated changes is generated by means of known patches with different shapes, sizes and change levels. Figs. 3 and 4 show the synthetic reflectivity images, without and with changes, and the ground truth maps of changes for the two datasets.

According to the flowchart in Fig. 1, Fig. 5 shows how simulated SLC images are generated starting from the synthetic reflectivity scenes, without or with changes. First the scene is multiplied by a spatial realization of a complex white Gaussian process, to yield the output of the SAR processor without focusing window. The sign introduced by the Gaussian noise makes the real and imaginary parts

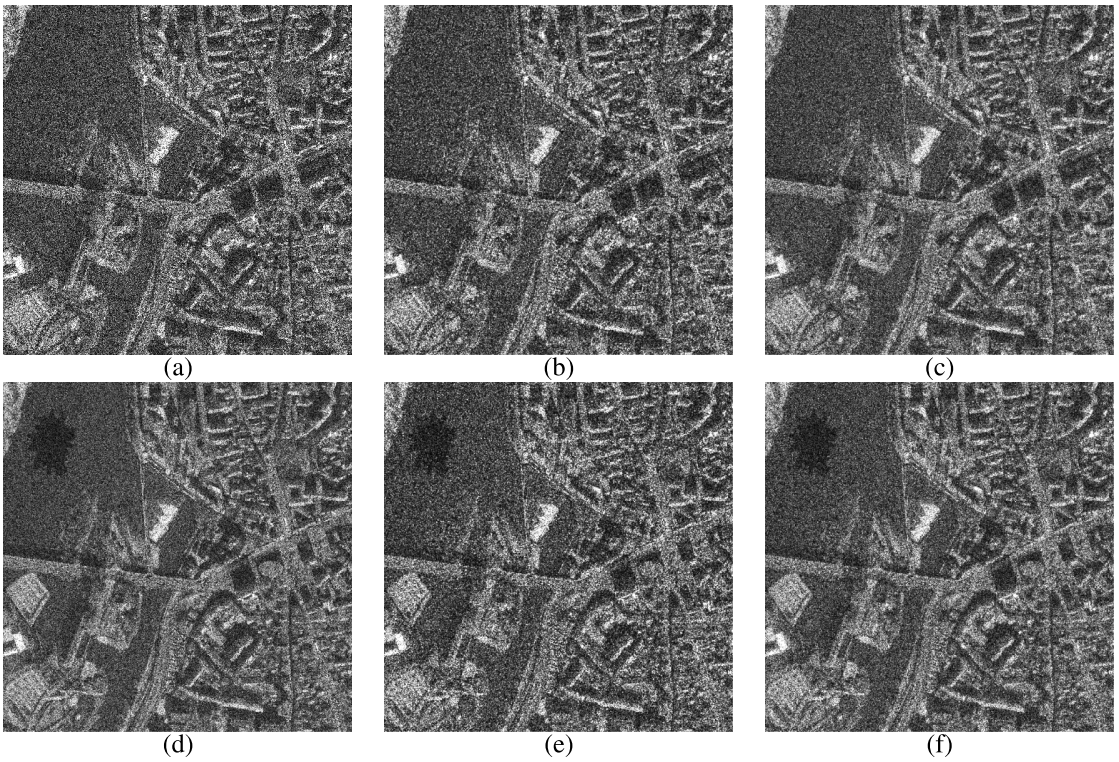

FIGURE 6. Dataset 1: Simulated pre-/post-event single-look amplitude images with; (a),(d) uncorrelated, (b),(e) correlated, (c),(f) decorrelated speckles.

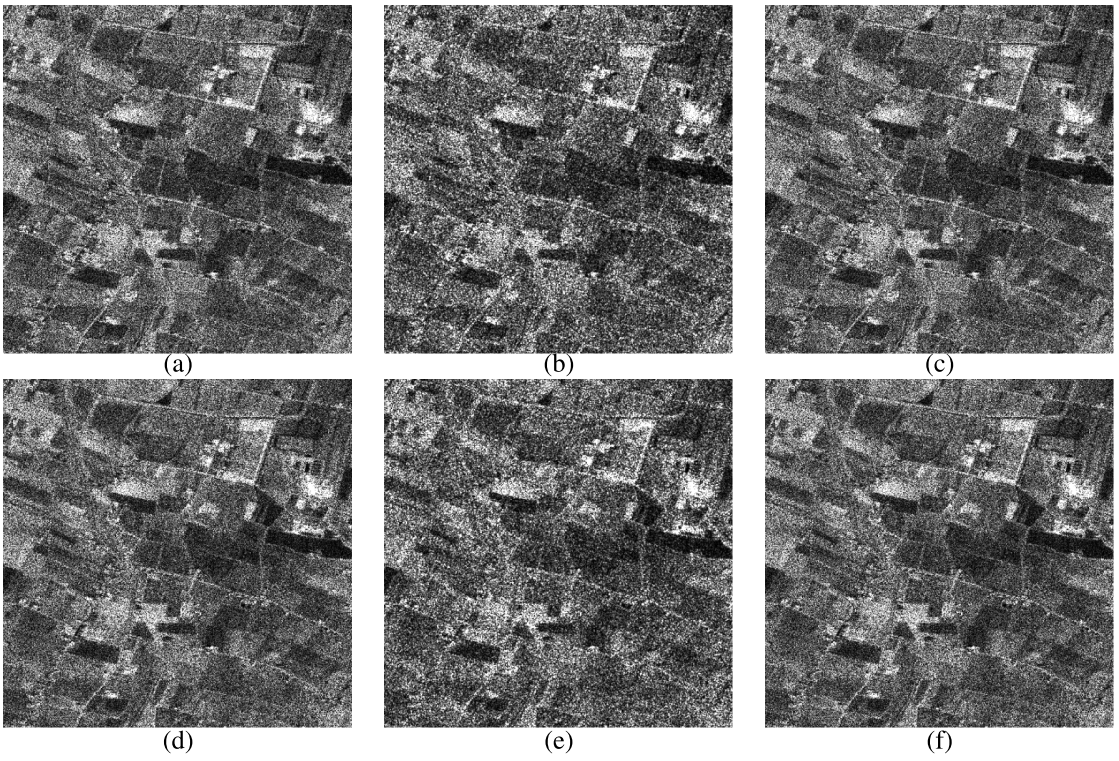

FIGURE 7. Dataset 2: Simulated pre-/post-event single-look amplitude images with; (a),(d) uncorrelated, (b),(e) correlated, (c),(f) decorrelated speckles.

of the synthetic SLC data to exactly fit the typical signed 12-bit format of true SLC data. The noise realizations of the pre-event and post-event scenes are obviously independent of one another. Then the Hamming frequency window is applied to the uncorrelated data, both real and imaginary parts, to produce an SLC image with spatially correlated

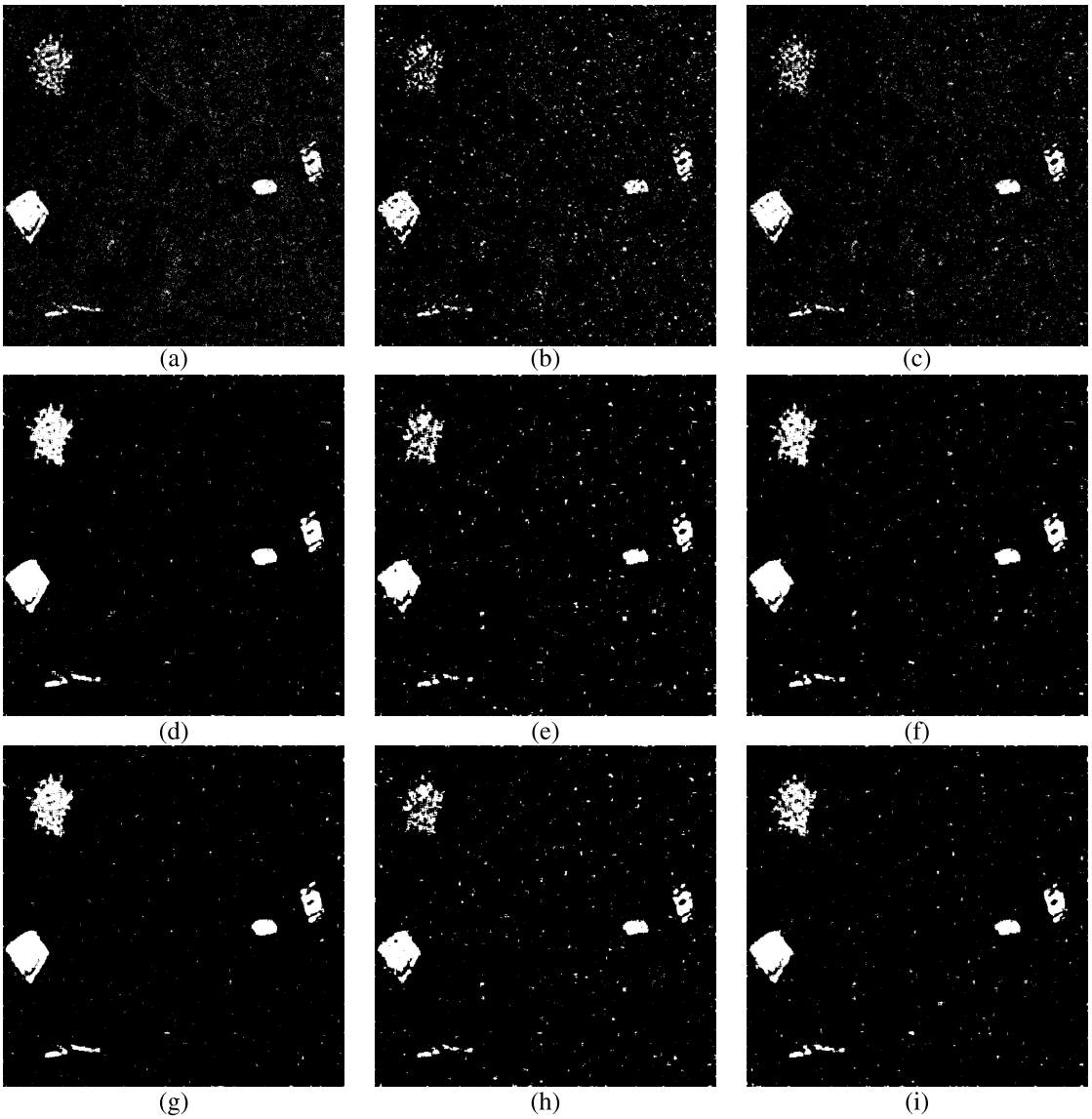

FIGURE 8. Dataset 1. Left column (a),(d),(g): uncorrelated; center column (b),(e),(h): correlated; right column (c),(f),(i): decorrelated. LR: (a)-(c); CKLD: (d)-(f); MS-ITCD: (g)-(i).

speckle. The original variance, which has been reduced by the filter, is restored, to avoid losing the calibration of the data. Eventually, the correlated image is whitened by means of the decorrelation procedure described in Section II [5]. Again the variance is adjusted to match its value before decorrelation. We wish to highlight that, even though the speckle is assumed to be fully developed and no processing of point targets is performed, this represents the least favorable case, because true targets are little noisy or no noisy at all; thus they are seldom mistaken by any change-detection algorithm. For other applications, like despeckling based on learning [46], different degrees of speckle development should be considered to train the network. In this case, the simulation of the dataset becomes a demanding task.

Figs. 6 and 7 show the synthetic single-look images for the two datasets, with uncorrelated, correlated and decorrelated speckle. Note that, while the grainy appearance of the correlated case stands out, the uncorrelated and decorrelated cases are almost identical. What immediately stand out is that all the images are extremely noisy and the change patches are hardly visible in some case. The subsequent analysis will demonstrate that, at the same SNR, the change analysis is significantly impaired by the speckle autocorrelation.

Three change-detection algorithms have been tested:

- Log-ratio (LR) preceded by despeckling (9×9 Kuan filtering [47]).
- Change analysis based on Kullback-Leibler distance (CKLD) [13].
- Mean-shift Information-Theoretic Change Detection (MS-ITCD) [14].

Thanks to the use of simulated data, the performance has been objectively evaluated by means of confusion matrices,

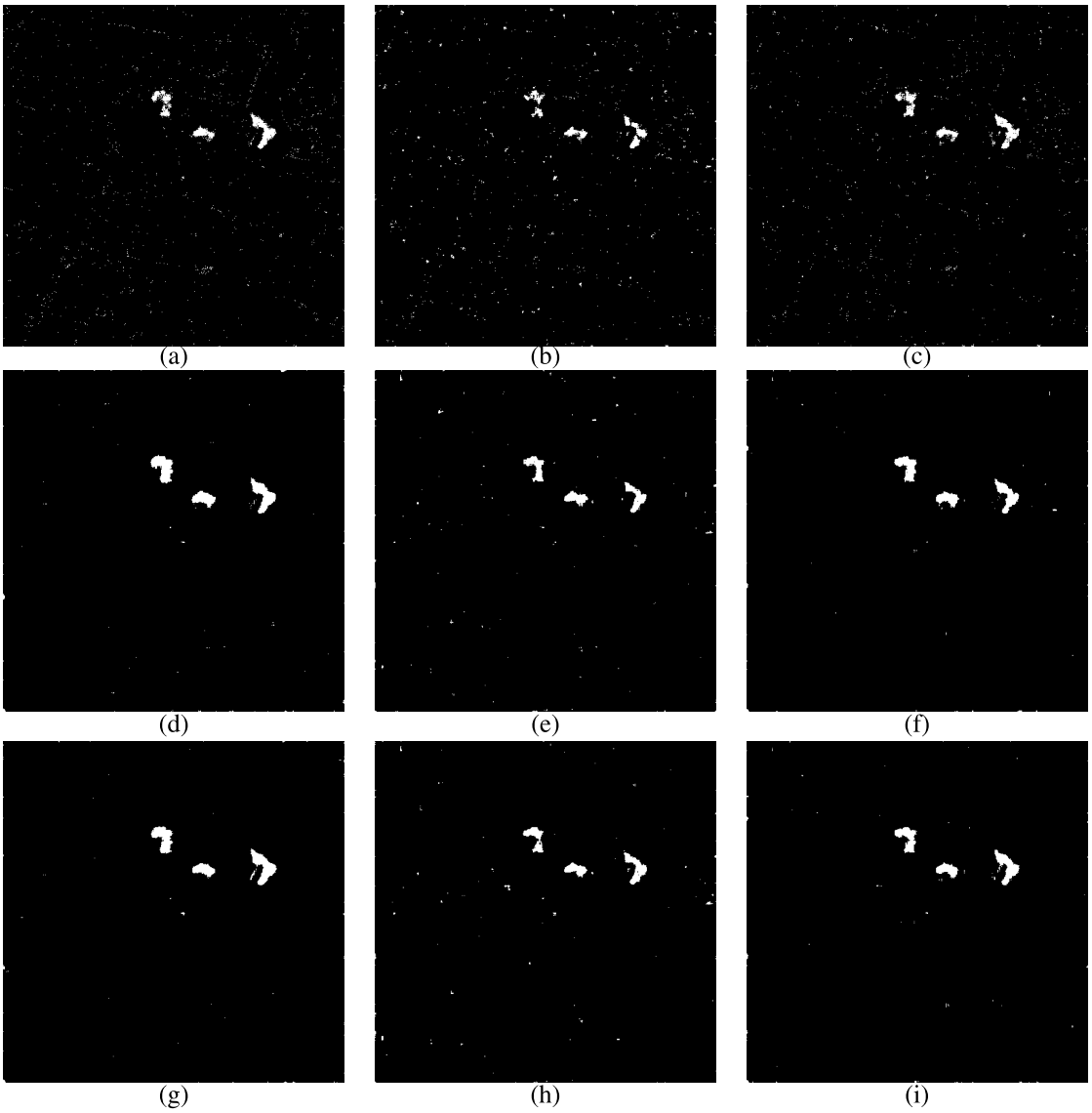

FIGURE 9. Dataset 2. Left column (a),(d),(g): uncorrelated; center column (b),(e),(h): correlated; right column (c),(f),(i): decorrelated. LR: (a)-(c); CKLD: (d)-(f); MS-ITCD: (g)-(i).

Receiver Operating Characteristic (ROC) curves and Area Under ROC Curve (AUC) metrics. Hereafter, the urban and rural datasets will be referred to as Dataset 1 and Dataset 2, respectively.

B. PERFORMANCE ANALYSIS

For each dataset, the three change algorithms have beer executed three times: a) with hypothetically uncorrelated speckle, which would require running the SAR processor without tapering window; b) with correlated speckle, as available with a standard SAR processor; c) with correlated speckle that has been de-correlated by the inverse filter [5], without processing of point targets because the synthetic speckle is fully developed.

Figs. 8 and 9 show change maps obtained by thresholding LR, CKLD and MS-ITCD features, respectively. For each change feature, thresholding has been performed by maximizing Cohen's kappa coefficient

$$\kappa = \frac{p_o - p_e}{1 - p_e} = 1 - \frac{1 - p_o}{1 - p_e}, \tag{14}$$

where p_o is the overall accuracy of the resulting change map and p_e is the accuracy of a random classifier.

For both the datasets and all algorithms, the uncorrelated cases (a),(d),(g) (leftmost column) are the best, in terms of lower number of false alarms (outliers) and geometric accuracy of patches. The correlated cases (b),(e),(h) (center column) is far the worst, especially in terms of number of outliers, which often occur also inside the patch, if the change level is low. The decorrelated cases (c),(f),(i) (rightmost column) is comparable to the uncorrelated cases. In the majority of real cases, the SAR raw data are slightly

oversampled to compensate the cutoff in bandwidth at the output of the SAR processor due to the tapering window.

The behaviors of the three algorithms is far different from one another. LR is not only the worst, but also the most sensitive to speckle correlation, also because the mandatory preliminary despeckling step is little effective on correlated 1-look data [5]. CKLD and MS-ITCD, though totally different to one another, perform similarly and much better than LR. CKLD is a bit more accurate in the uncorrelated case, but MS-ITCD is better in the decorrelated case. The latter is especially robust to speckle in general, as otherwise noticed since its introduction [14]. Thus, even though both are geometrically accurate, MS-ITCD produces a lower number of false alarms, in general. The considerations on the change maps in Fig. 8 are strengthened by the maps in Fig. 9 relative to the less challenging rural landscape.

To each of the simulations shown in Figs. 8 and 9 a confusion matrix is associated. A synoptic view of each confusion matrix [34] is represented by κ (14), which ranges in [0,1] and is independent of the population of each class, far different for changed and unchanged pixels. Table 1 report the kappa coefficients of all the 18 simulations (2 datasets $\times$ 3 change algorithms $\times$ 3 cases of correlation). What immediately stands out is that LR preceded by despekling is moderately sensitive to correlation but also the least performing method. CKLD is top performing, but extremely sensitive to correlation. MS-ITCD best trades off insensitivity to correlation and detection ability. Dataset 2 presents higher values of κ, being more likely as a true SAR image, because speckle is not always fully developed on an urban landscape. In other works, Dataset 1 is too noisy because, in a true SAR image, a built area made of man-made scatterers is much less noisy than in the simulated fully developed case.

Fig. 10 shows the ROC curve representing the change discrimination capability, that is, the True Positive Rate (TPR) versus the False Positive Rate (FPR), of the LR algorithm, for the three cases of speckle correlation. Each point of a ROC curve corresponds to a decision threshold to detect changes and determines TPR and FPR values. The threshold maximizing κ corresponds to the point on the ROC curve that minimizes the distance from the point (TPR=1,FPR=0), the upper-left vertex of the ROC plane. Though LR is a point operator and should be not affected, at least in principle, by spatial correlation, the decorrelation is beneficial because LR is very sensitive to the noise and requires a preliminary despeckling stage, which is sensitive to correlation, at least if local operators are used [20]. The loss of bandwidth with respect to the uncorrelated case is negligible, also because such a loss is lower than that introduced by the de-speckling stage.

Fig. 11 shows the ROC performance of the CKLD varying with the type of speckle. Again, the usefulness of decorrelation stands out. Unlike what happens for LR, the uncorrelated case is slightly more favorable than the decorrelated case, presumably because now there is no preliminary despeckling. However, the parametric model of the data, on which CKLD relies, still seems to benefit from the missing spatial correlation of speckle.

TABLE 1. Kappa coefficient of simulations in Figs. 8 and 9.

Dataset 1	uncorrelated	correlated	decorrelated
LR	0.5665	0.4853	0.5590
CKLD	0.8427	0.6684	0.7708
MS-ITCD	0.8374	0.6692	0.7659
Dataset 2	uncorrelated	correlated	decorrelated
LR	0.5808	0.4574	0.5796
CKLD	0.8124	0.6774	0.7812
MS-ITCD	0.8445	0.7001	0.8020

TABLE 2. Areas underlying ROC curves for different change algorithms and correlations.

Dataset 1	uncorrelated	correlated	decorrelated
LR	0.9572	0.9247	0.9527
CKLD	0.9817	0.9476	0.9728
MS-ITCD	0.9726	0.9565	0.9658
Dataset 2	uncorrelated	correlated	decorrelated
LR	0.9818	0.9607	0.9788
CKLD	0.9921	0.9661	0.9859
MS-ITCD	0.9913	0.9670	0.9862

Fig. 12 shows that also the nonparametric method based on mean-shift clustering of local means takes a significant advantage of the uncorrelatedness of speckle. In fact, the estimates of local statistics are more accurate if the noise is white. In the decorrelated case, the loss of bandwidth practically does not affect the performance, because the local mean can be regarded as the results of a spatial filter, same as despeckling for LR.

Eventually, the discrimination capability of the three change features is summarized in Table 2 for the two datasets. The area underlying the ROC curve, which should ideally tend to one, highlights the loss of performance due to correlation. The decorrelated case is a fair approximation of the ideal uncorrelated case, which is unfeasible if focusing of targets is crucial. Overall, LR is poorer, while CKLD and MS-ITCD are pretty equivalent in performance to one another, regardless of correlation. For the ideal case of uncorrelated speckle, CKLD is the best method for Dataset 1; MS-ITCD for Dataset 2. In the case of correlated speckle, MS-ITCD is the best method for both the datasets, though marginally on Dataset 1. For decorrelated speckle, CKLD is slightly better on Dataset 1; MS-ITCD superior on Dataset 2.

C. DISCUSSION

The spatial correlation of speckle, introduced by the SAR processor to improve the focusing of point targets, has a series of undesired consequences on the subsequent processing for SNR improvement and information extraction from SLC data: i) a decrement in the performance of despeckling methods, which usually assume uncorrelated noise [5]; ii) an inaccurate interferometric coherence, whose estimation is biased in excess depending on the amount of (auto)correlation [6], unless nonlocal algorithms are

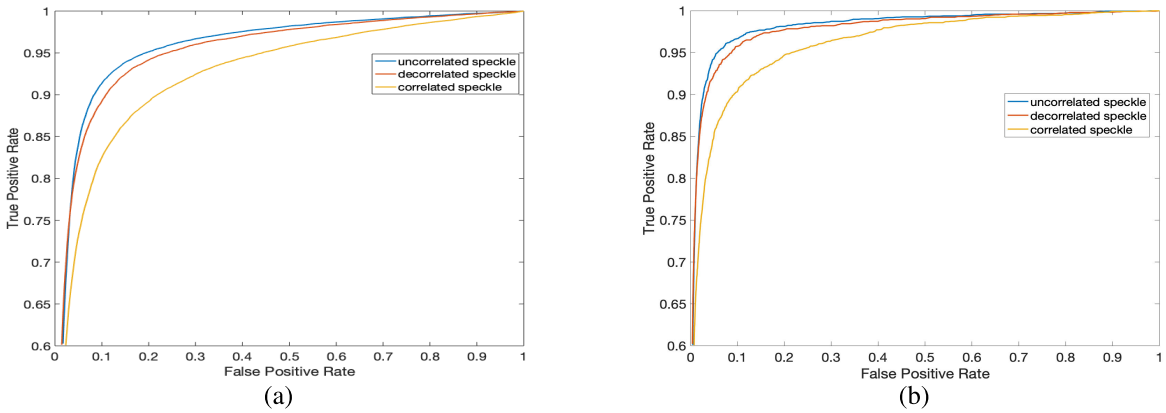

FIGURE 10. ROC cuves for LR: (a) Dataset 1; (b) Dataset 2.

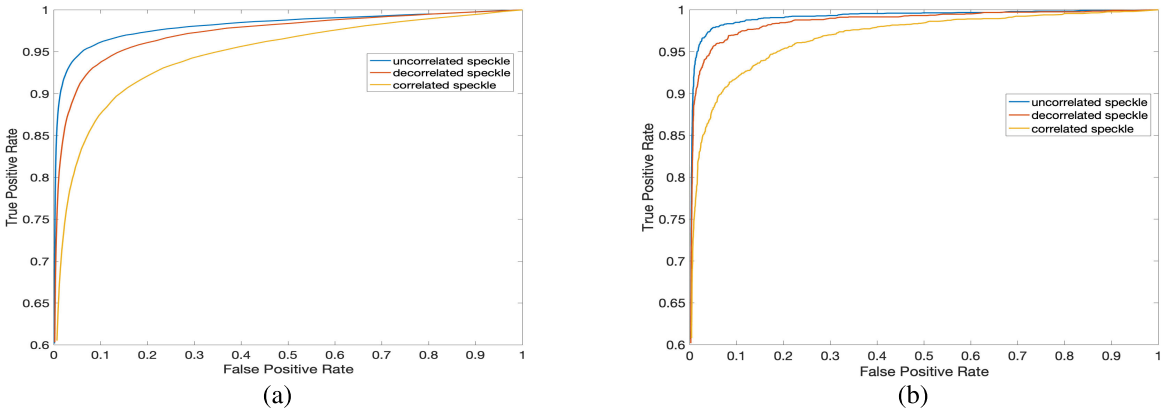

FIGURE 11. ROC cuves for CKLD: (a) Dataset 1; (b) Dataset 2.

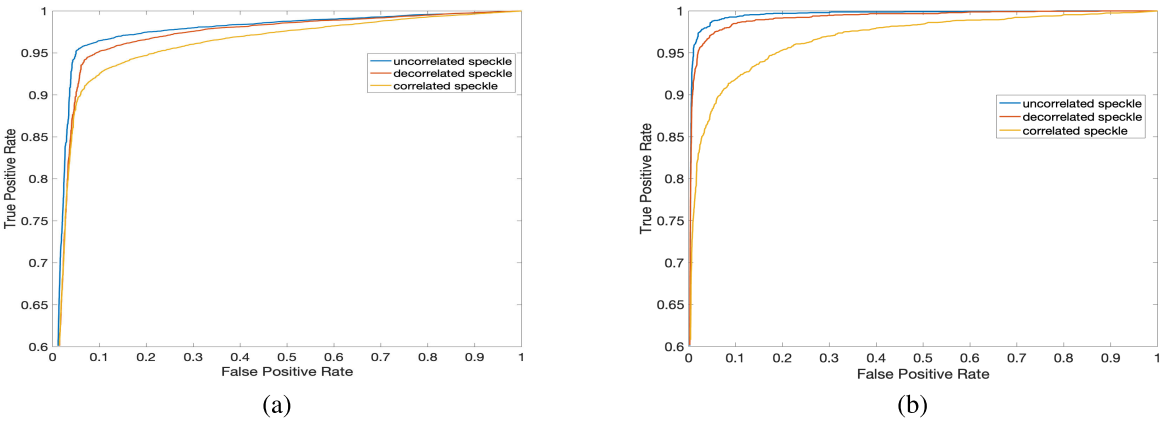

FIGURE 12. ROC curves for MS-ITCD: (a) Dataset 1; (b) Dataset 2.

used [48]; iii) a reduced accuracy in the estimation of polarimetric features [10].

When the SLC data are envelope-detected and multi-looked, the spatial correlation is maximum for single-look data and decreases for increasing number of looks. The present study has demonstrated that, whenever the change detection task is carried out on single-look data, the spatial correlation should be preliminarily removed. If the despeckling or change detection task are performed on incoherently multilooked (real) data, the spatial correlation is mitigated by the downsampling [5]; thus, the spatial decorrelation, which would be unfeasible on envelope-detected data, is no longer necessary.

The introduction of a preliminary decorrelation stage of the SLC data is found to significantly improve the accuracy of change detection, as performed on the modulus of the SLC images by different parametric and nonparametric algorithms. Tests on simulated SLC images, with synthetic fully-developed speckle, show that the change detection capability of decorrelated data is significantly better than that of the correlated data that are available at the output of the SAR processor. The proposed system closely attains the ultimate performance, which can be achieved only in the case of perfectly white speckle; an ideal case, because of the small loss of bandwidth originated by the slight oversampling of raw data. Again, we wish to remark that the case of fully-developed speckle, easily available for simulation purposes, represents the worst case in terms of SNR of the data. In practical cases, in which point targets and strong scatterers are removed and reinserted after the whitening, the average noisiness of the data will be lower and hence the estimation accuracy of change is expected to be greater.

The computational complexity of the whitening process, including processing of point targets, is one order of magnitude lower than that of the subsequent change-detection algorithms, at least for CKLD and MS-ITCD, which are computationally comparable. Actually, MS-ITCD is much faster, if a binned implementation of MS is used. LR is faster, at least if the preliminary despeckling step is not too sophisticated. In this study, we adopted the simple and fast Kuan's despeckling filter [47], that is, a local linear minimum mean square error (LLMMSE) estimator in the spatial domain. As shown in [14], however, the majority of de-speckling algorithms takes advantage of the uncorrelatedness of speckle. Thus, the proposed whitening patch improves the de-speckling performance and hence that of LR change detection relying on de-speckling. Note that, for CKLD e MS-ITCD, de-speckling does not improve the detection of changes [13], [14]. With a more advanced de-speckling stage, possibly less sensitive to correlation, however, it is hard to believe that LR might ever fill the gap in performance towards the other two change detection algorithms.

V. CONCLUSION

In SAR remote sensing applications, whenever the spatial resolution of the data is crucial, multilook products may be unfit. In this case, SLC products, which retain the full resolution of the system and are usually not geocoded, may be invaluable. If a couple of SLC images of the same scene is available, an analysis of interferometric coherence may be integrated with an analysis of structural changes of backscatter. Unfortunately, SLC data are extremely noisy and are affected by spatially correlated noise. Hence, backscatter analysis and information extraction tools may become little performing. This is the main reason, for which SLC data are mainly used for interferometric applications and less frequently for change analysis of backscatter.

This study has highlighted that change analysis from SLC data is found to benefit from a preliminary decorrelation of speckles. The benefits of speckle decorrelation is twofold: on one side, the geometric accuracy of the changed patches is increased, thanks to the full resolution of the SAR system; on the other side, the number of outliers, or false alarms, is significantly reduced, thanks to the whiteness of speckle. The false-alarm rate may be further abated by means of a contextual analysis of changes, with the risk of suppressing true changes of small size, which would be mistaken for outliers. For this reason, in this study, no contextual analysis of changes has been performed.

The proposed decorrelation procedure of SLC data is expected to increase the performance of SAR change detection methods that use phase information [49], [50].

A further application of the decorrelation procedure [5] may concern an analysis of the impact of a spatial decorrelation of SLC data on the SAR tomographic processing [51]. In this case, phase information is crucial and the SLC format should be extremely accurate.

ACKNOWLEDGMENT

The authors would like to thank the contribution of their former coauthors, Bruno Aiazzi, who prematurely passed away, in 2021, and Claudia Zoppetti, who recently started a promising activity of technological transfer.

REFERENCES

[1] C. Oliver and S. Quegan, *Understanding Synthetic Aperture Radar Images* (The SciTech Radar and Defense Series). Raleigh, NC, USA: SciTech Publishing Inc., 2004.

[2] S. Solbo and T. Eltoft, "A stationary wavelet-domain Wiener filter for correlated speckle," *IEEE Trans. Geosci. Remote Sens.*, vol. 46, no. 4, pp. 1219–1230, Apr. 2008.

[3] S. Foucher, J.-M. Boucher, and G. B. Benie, "Wavelet filtering of correlated speckle," *Proc. SPIE*, vol. 5108, pp. 307–316, Aug. 2003.

[4] A. Moreira, P. Prats-Iraola, M. Younis, G. Krieger, I. Hajnsek, and K. P. Papathanassiou, "A tutorial on synthetic aperture radar," *IEEE Geosci. Remote Sens. Mag.*, vol. 1, no. 1, pp. 6–43, Mar. 2013.

[5] A. Lapini, T. Bianchi, F. Argenti, and L. Alparone, "Blind speckle decorrelation for SAR image despeckling," *IEEE Trans. Geosci. Remote Sens.*, vol. 52, no. 2, pp. 1044–1058, Feb. 2014.

[6] F. Sica, L. Alparone, F. Argenti, G. Fornaro, A. Lapini, and D. Reale, "Benefits of blind speckle decorrelation for InSAR processing," *Proc. SPIE*, vol. 9243, pp. 98–105, Oct. 2014.

[7] R. Touzi, A. Lopes, J. Bruniquel, and P. W. Vachon, "Coherence estimation for SAR imagery," *IEEE Trans. Geosci. Remote Sens.*, vol. 37, no. 1, pp. 135–149, Jan. 1999.

[8] B. Aiazzi, L. Alparone, S. Baronti, and A. Garzelli, "Coherence estimation from multilook incoherent SAR imagery," *IEEE Trans. Geosci. Remote Sens.*, vol. 41, no. 11, pp. 2531–2539, Nov. 2003.

[9] A. Arienzo, F. Argenti, and L. Alparone, "Impact of a spatial decorrelation of the noise on the performance of despeckling filters for polarimetric SAR data," in *Proc. Photon. Electromagn. Res. Symp.*, Jun. 2019, pp. 1113–1121.

[10] A. Arienzo, F. Argenti, L. Alparone, and M. Gherardelli, "Accurate despeckling and estimation of polarimetric features by means of a spatial decorrelation of the noise in complex PolSAR data," *Remote Sens.*, vol. 12, no. 2, p. 331, Jan. 2020. [Online]. Available: https://www.mdpi.com/2072-4292/12/2/331

[11] A. Garzelli, B. Aiazzi, L. Alparone, F. Argenti, A. Arienzo, and C. Zoppetti, "Impact of a spatial decorrelation of the noise on the estimation accuracy of temporal changes in the scene from a couple of single-look SAR images," *Proc. SPIE*, vol. 11533, pp. 107–117, May 2020, doi: 10.1117/12.2574601.

[12] A. Garzelli and C. Zoppetti, "Optimizing SAR change detection based on log-ratio features," in *Proc. 9th Int. Workshop Anal. Multitemporal Remote Sens. Images (MultiTemp)*, Jun. 2017, pp. 1–4.

[13] J. Inglada and G. Mercier, "A new statistical similarity measure for change detection in multitemporal SAR images and its extension to multiscale change analysis," *IEEE Trans. Geosci. Remote Sens.*, vol. 45, no. 5, pp. 1432–1445, May 2007.

[14] B. Aiazzi, L. Alparone, S. Baronti, A. Garzelli, and C. Zoppetti, "Nonparametric change detection in multitemporal SAR images based on mean-shift clustering," *IEEE Trans. Geosci. Remote Sens.*, vol. 51, no. 4, pp. 2022–2031, Apr. 2013.

[15] A. Garzelli and C. Zoppetti, "Geometrically accurate change mapping from vhr SAR images," in *Proc. IGARSS - IEEE Int. Geosci. Remote Sens. Symp.*, Jul. 2019, pp. 25–28.

[16] B. Aiazzi, F. Bovolo, L. Bruzzone, A. Garzelli, D. Pirrone, and C. Zoppetti, *Change Detection in Multitemporal Images Through Single- and Multi-scale Approaches*. Cham, Switzerland: Springer, 2018, pp. 325–355.

[17] F. Argenti and L. Facheris, "Radar pulse compression methods based on nonlinear and quadratic optimization," *IEEE Trans. Geosci. Remote Sens.*, vol. 59, no. 5, pp. 3904–3916, May 2021.

[18] L. Miccinesi, A. Beni, and M. Pieraccini, "UAS-borne radar for remote sensing: A review," *Electronics*, vol. 11, no. 20, p. 3324, Oct. 2022. [Online]. Available: https://www.mdpi.com/2079-9292/11/20/3324

[19] S. Madsen, "Spectral properties of homogeneous and nonhomogeneous radar images," *IEEE Trans. Aerosp. Electron. Syst.*, vol. AES-23, no. 4, pp. 583–588, Jul. 1987.

[20] T. Bianchi, F. Argenti, A. Lapini, and L. Alparone, "Amplitude vs intensity Bayesian despeckling in the wavelet domain for SAR images," *Digit. Signal Process.*, vol. 23, no. 5, pp. 1353–1362, Sep. 2013.

[21] C. Lopez-Martinez and X. Fabregas, "Polarimetric SAR speckle noise model," *IEEE Trans. Geosci. Remote Sens.*, vol. 41, no. 10, pp. 2232–2242, Oct. 2003.

[22] A. Lopes, R. Touzi, and E. Nezry, "Adaptive speckle filters and scene heterogeneity," *IEEE Trans. Geosci. Remote Sens.*, vol. 28, no. 6, pp. 992–1000, Mar. 1990.

[23] A. Freeman, "SAR calibration: An overview," *IEEE Trans. Geosci. Remote Sens.*, vol. 30, no. 6, pp. 1107–1121, Jun. 1992.

[24] G. Gao, "Statistical modeling of SAR images: A survey," *Sensors*, vol. 10, no. 1, pp. 775–795, Jan. 2010. [Online]. Available: https://www.mdpi.com/1424-8220/10/1/775

[25] A. Lapini, S. Pettinato, E. Santi, S. Paloscia, G. Fontanelli, and A. Garzelli, "Comparison of machine learning methods applied to SAR images for forest classification in Mediterranean areas," *Remote Sens.*, vol. 12, no. 3, p. 369, Jan. 2020. [Online]. Available: https://www.mdpi.com/2072-4292/12/3/369

[26] E. J. M. Rignot and J. J. van Zyl, "Change detection techniques for ERS-1 SAR data," *IEEE Trans. Geosci. Remote Sens.*, vol. 31, no. 4, pp. 896–906, Jul. 1993.

[27] L. Gomez, R. Ospina, and A. Frery, "Statistical properties of an unassisted image quality index for SAR imagery," *Remote Sens.*, vol. 11, no. 4, p. 385, Feb. 2019.

[28] F. Argenti, A. Lapini, T. Bianchi, and L. Alparone, "A tutorial on speckle reduction in synthetic aperture radar images," *IEEE Geosci. Remote Sens. Mag.*, vol. 1, no. 3, pp. 6–35, Sep. 2013.

[29] F. Argenti, G. Torricelli, and L. Alparone, "MMSE filtering of generalised signal-dependent noise in spatial and shift-invariant wavelet domains," *Signal Process.*, vol. 86, no. 8, pp. 2056–2066, Aug. 2006.

[30] F. Argenti, T. Bianchi, and L. Alparone, "Multiresolution MAP despeckling of SAR images based on locally adaptive generalized Gaussian pdf modeling," *IEEE Trans. Image Process.*, vol. 15, no. 11, pp. 3385–3399, Nov. 2006.

[31] T. Bianchi, F. Argenti, and L. Alparone, "Segmentation-based MAP despeckling of SAR images in the undecimated wavelet domain," *IEEE Trans. Geosci. Remote Sens.*, vol. 46, no. 9, pp. 2728–2742, Sep. 2008.

[32] F. Argenti, T. Bianchi, A. Lapini, and L. Alparone, "Fast MAP despeckling based on Laplacian–Gaussian modeling of wavelet coefficients," *IEEE Geosci. Remote Sens. Lett.*, vol. 9, no. 1, pp. 13–17, Jan. 2012.

[33] B. Aiazzi, L. Alparone, and S. Baronti, "Information-theoretic heterogeneity measurement for SAR imagery," *IEEE Trans. Geosci. Remote Sens.*, vol. 43, no. 3, pp. 619–624, Mar. 2005.

[34] C. D'Elia, S. Ruscino, M. Abbate, B. Aiazzi, S. Baronti, and L. Alparone, "SAR image classification through information-theoretic textural features, MRF segmentation, and object-oriented learning vector quantization," *IEEE J. Sel. Topics Appl. Earth Observ. Remote Sens.*, vol. 7, no. 4, pp. 1116–1126, Apr. 2014.

[35] L. Alparone, L. Facheris, S. Baronti, A. Garzelli, and F. Nencini, "Fusion of multispectral and SAR images by intensity modulation," in *Proc. Procs. 7th Int. Conf. Inform. Fusion*, vol. 2, 2004, p. 637.

[36] B. Aiazzi, L. Alparone, A. Arienzo, A. Garzelli, and C. Zoppetti, "Monitoring of changes in vegetation status through integration of time series of hyper-sharpened Sentinel-2 red-edge bands and information-theoretic textural features of Sentinel-1 SAR backscatter," *Proc. SPIE*, vol. 11155, Jul. 2019, Art. no. 111550z.

[37] L. Alparone, A. Arienzo, A. Garzelli, S. Lolli, and C. Zoppetti, "Fusion of optical and SAR satellite data for environmental monitoring: Assessment of damages and disturbances originated by forest fires," *Proc. SPIE*, vol. 12267, Nov. 2022, Art. no. 122670E, doi: 10.1117/12.2638984.

[38] L. Alparone, A. Garzelli, and C. Zoppetti, "Fusion of VNIR optical and C-band polarimetric SAR satellite data for accurate detection of temporal changes in vegetated areas," *Remote Sens.*, vol. 15, no. 3, pp. 638-1–638-18, 2023. [Online]. Available: https://www.mdpi.com/2072-4292/15/3/638

[39] F. T. Ulaby, F. Kouyate, B. Brisco, and T. H. L. Williams, "Textural information in SAR images," *IEEE Trans. Geosci. Remote Sens.*, vol. GRS-24, no. 2, pp. 235–245, Mar. 1986.

[40] F. Bujor, E. Trouve, L. Valet, J.-M. Nicolas, and J.-P. Rudant, "Application of log-cumulants to the detection of spatiotemporal discontinuities in multitemporal SAR images," *IEEE Trans. Geosci. Remote Sens.*, vol. 42, no. 10, pp. 2073–2084, Oct. 2004.

[41] M. Gong, Y. Cao, and Q. Wu, "A neighborhood-based ratio approach for change detection in SAR images," *IEEE Geosci. Remote Sens. Lett.*, vol. 9, no. 2, pp. 307–311, Mar. 2012.

[42] D. Comaniciu and P. Meer, "Mean shift: A robust approach toward feature space analysis," *IEEE Trans. Pattern Anal. Mach. Intell.*, vol. 24, no. 5, pp. 603–619, May 2002.

[43] B. Aiazzi, L. Alparone, S. Baronti, A. Garzelli, and C. Zoppetti, "A robust change detection feature for cosmo-SkyMed detected SAR images," in *Proc. 6th Int. Workshop Anal. Multi-Temporal Remote Sens. Images*, Jul. 2011, pp. 125–128.

[44] B. Aiazzi, L. Alparone, S. Baronti, A. Garzelli, and F. Nencini, "Information-theoretic multitemporal features for change analysis from SAR images," *Proc. SPIE*, vol. 7109, Feb. 2008, Art. no. 71090S.

[45] A. D. C. Nascimento, A. C. Frery, and R. J. Cintra, "Detecting changes in fully polarimetric SAR imagery with statistical information theory," *IEEE Trans. Geosci. Remote Sens.*, vol. 57, no. 3, pp. 1380–1392, Mar. 2019.

[46] F. Lattari, B. Gonzalez Leon, F. Asaro, A. Rucci, C. Prati, and M. Matteucci, "Deep learning for SAR image despeckling," *Remote Sens.*, vol. 11, no. 13, p. 1532, Jun. 2019.

[47] D. T. Kuan, A. A. Sawchuk, T. C. Strand, and P. Chavel, "Adaptive noise smoothing filter for images with signal-dependent noise," *IEEE Trans. Pattern Anal. Mach. Intell.*, vol. PAMI-7, no. 2, pp. 165–177, Mar. 1985.

[48] C.-A. Deledalle, L. Denis, F. Tupin, A. Reigber, and M. Jäger, "NL-SAR: A unified nonlocal framework for resolution-preserving (Pol)(In)SAR denoising," *IEEE Trans. Geosci. Remote Sens.*, vol. 53, no. 4, pp. 2021–2038, Apr. 2015.

[49] W. L. Hakim, A. R. Achmad, J. Eom, and C.-W. Lee, "Land subsidence measurement of Jakarta coastal area using time series interferometry with Sentinel-1 SAR data," *J. Coastal Res.*, vol. 102, no. 1, pp. 75–81, Dec. 2020, doi: 10.2112/si102-010.1.

[50] M. Kang and J. Baek, "SAR image change detection via multiple-window processing with structural similarity," *Sensors*, vol. 21, no. 19, p. 6645, Oct. 2021. [Online]. Available: https://www.mdpi.com/1424-8220/21/19/6645

[51] F. Lombardini and F. Cai, "Generalized-capon method for diff-tomo SAR analyses of decorrelating scatterers," *Remote Sens.*, vol. 11, no. 4, p. 412, Feb. 2019.

LUCIANO ALPARONE received the Laurea (M.Sc.) degree (Hons.) in electronic engineering from the University of Florence, Florence, Italy, in 1985, and the Ph.D. degree in telecommunications and information science from Italian Ministry of Education, University and Research, in 1990.

Since 2002, he has been an Associate Professor with the Department of Information Engineering (DINFO, after 2011), University of Florence. He is currently a Full Professor in telecommunications and the Head of the Signal Processing and Telecommunications Laboratory. (LENST). He has authored or coauthored about 100 articles in peer-reviewed journals and a total of more than 300 publications. His research interests include data compression for remote sensing applications, multiresolution image analysis and processing, multisensor image fusion, analysis, and processing of SAR images.

Dr. Alparone was a co-recipient of the 2004 IEEE Geoscience and Remote Sensing Letters Prize Paper Award for the study on "A global quality measurement of pansharpened multispectral imagery." He has been the principal author of the book *Remote Sensing Image Fusion* (CRC Press, Taylor & Francis Group, Boca Raton, FL, USA, March 2015). He is listed in both career-long and single-year (2019 onward) world's top 2% scientists by Stanford University.

FABRIZIO ARGENTI (Senior Member, IEEE) received the Laurea degree (cum laude) in electronics engineering and the Ph.D. degree in electronics and information engineering from the University of Florence, Florence, Italy, in 1989 and 1993, respectively. Since 1993, he has been with the Department of Electronics and Telecommunications (now Department of Information Engineering), University of Florence, where he was an Assistant Professor and then has been an Associate Professor, since 2002. His teaching experience includes courses on digital signal processing, estimation theory, and information theory. He has been involved in several research projects in the fields of image processing, multimedia transmission, and remote sensing. His research interests include image processing, multiresolution analysis, statistical signal processing, remote sensing, inverse problems, and machine learning approaches to signal processing.

ALBERTO ARIENZO received the B.S. and M.S. degrees in telecommunications engineering and the Ph.D. degree in information engineering from the University of Florence, Italy, in 2012, 2015, and 2023, respectively. From 2018 to 2022, he was with the Institute of Applied Physics Nello Carrara IFAC-CNR, National Research Council of Italy. Since 2023, he has been with OHB System AG, Oberpfaffenhofen, Germany, as a Performance and Calibration System Engineer in electro-optical sensors. His research and professional interests include remote sensing, imagery science, and multisensor data fusion.

ANDREA GARZELLI (Senior Member, IEEE) received the Laurea degree (summa cum laude) in electronic engineering and the Ph.D. degree in information and telecommunications engineering from the University of Florence, Italy, in 1991 and 1995, respectively.

He is currently a Professor in telecommunications with the Department of Information Engineering and Mathematics, University of Siena, Italy, where he holds the courses of fundamentals of signal processing and telecommunications, statistical signal processing, and remote sensing. He has coauthored the book *Remote Sensing Image Fusion* (CRC Press, 2015). His research interests include image analysis and classification with applications to image fusion for optical and synthetic aperture radar images.

Dr. Garzelli is a member of the IEEE Geoscience and Remote Sensing Society. He was a co-recipient of the IEEE Geoscience and Remote Sensing Letters Prize Paper Award, in 2004. He was a recipient of the recognition of best reviewers of the IEEE TRANSACTIONS ON GEOSCIENCE AND REMOTE SENSING, in 2014, a journal for which he has been an Associate Editor, since 2015. He is listed in the world's top 2% scientists by Stanford University, in 2019, 2020, 2021, and 2022, and for the entire career.

Open Access funding provided by 'Università degli Studi di Firenze' within the CRUI CARE Agreement